FRET Visualization of High Mechanosensation of von Willebrand Factor to Hydrodynamic Force

Mingxing Ouyang *, Yao Gao, Binqian Zhou, Jia Guo, Lei Lei, Yingxiao Wang, Linhong Deng *

Posted Date: 13 February 2025

doi: 10.20944/preprints202502.0915.v1

Keywords: von Willebrand factor; fluid shear; Förster resonance energy transfer (FRET); mechanosensation; molecular unfolding; hemophilia

 doi:10.20944/preprints202502.0915.v1

Article

FRET Visualization of High Mechanosensation of von Willebrand Factor to Hydrodynamic Force

Mingxing Ouyang [1,*,#], Yao Gao [1,2,#], Binqian Zhou [1,2], Jia Guo [1], Lei Lei [3], Yingxiao Wang [3,4] and Linhong Deng [1,*]

[1] Institute of Biomedical Engineering and Health Sciences, School of Medical and Health Engineering, Changzhou University, Changzhou, Jiangsu Province 213164 China

[2] School of Pharmacy, Changzhou University, Changzhou, Jiangsu Province 213164 China

[3] Shu Chien-Gene Lay Department of Bioengineering, and Institute of Engineering in Medicine, University of California at San Diego, La Jolla, CA 92093 USA

[4] Alfred E. Mann Department of Biomedical Engineering, University of Southern California, Los Angeles, CA 90089 USA

* Correspondence: mxouyang@cczu.edu.cn (M.O.); dlh@cczu.edu.cn (L.D.)

[#] M.O. and Y.G. share the first authorships.

Abstract: von Willebrand factor (vWF) is a large glycoprotein in circulation system, which senses hydrodynamic force at vascular injuries and then recruits platelets in assembling clots. How vWF mechanosenses shear flow for molecular unfolding is an important topic. Here, Förster resonance energy transfer (FRET) biosensor was developed to monitor vWF conformation change to hydrodynamic force. The full-length vWF-based biosensor is anchored on cell surface, in which A2 domain is flanked with FRET pair. With 293T cells seeded into microfluidic channels, 2.8 dyn/cm^2 shear force induced remarkable FRET change (~60%) in 30 min. Gradient micro-shear below 2.8 dyn/cm^2 demonstrated FRET responses positively related to flow magnitudes with 0.14 dyn/cm^2 inducing obvious change (~16%). The FRET increases indicate closer positioning of A2's two termini in vWF, supported with high FRET of A2 only-based biosensor, which probably resulted from flow-induced A2 dissociation from vWF intramolecular binding. Interestingly, gradual increase of flow from 2.8 to 28 dyn/cm^2 led to decreasing FRET changes, suggesting the second-level unfolding in A2 domain. LOCK-vWF biosensor with bridged A2 two termini or A2 only biosensor couldn't sense the shear, indicating structure-flexible A2 and large vWF molecules important in the mechanosensation. In conclusion, the developed vWF-based biosensor demonstrated high mechanosensation of vWF with two-level unfolding to shear force: the dissociation of A2 domain from vWF intramolecular binding under micro shear, and then unfolding of A2 in vWF under higher shear. This study provides new insights on vWF mechanosensitive feature for its physiological functions and implicated disorders.

Keywords: von Willebrand factor; fluid shear; Förster resonance energy transfer (FRET); mechanosensation; molecular unfolding; hemophilia

1. Introduction

Hemophilia is a hereditary bleeding disorder caused by deficiency or abnormal function of coagulation factors[1–3]. Under normal conditions, when a blood vessel is damaged, coagulation factors are activated and form a thrombus, thus preventing bleeding. However, in hemophiliacs, the synthesis or function of coagulation factors is affected due to mutations in specific coagulation factor genes[4,5]. von Willebrand disease (vWD) is a common disorder among hemophiliacs and caused by insufficient amount or abnormal function of von Willebrand factor (vWF) in plasma[6,7]. vWF is a

 doi:10.20944/preprints202502.0915.v1

macromolecular glycoprotein, which gene is located on human chromosome 12, containing 52 exons and 51 introns, and these exons encode the different structural domains of the vWF protein[8,9].

The most common types of mutations in vWD are point mutations which may result in structural abnormalities or impaired function of the vWF protein[10]. For example, some point mutations may lead to increased cleavage of the vWF protein, thereby reducing its concentration in the blood, while others may affect the ability of the vWF protein to bind to platelets and coagulation factor VIII, thereby affecting the blood coagulation process [11,12]. Large deletion or insertion mutations may also lead to complete or partial deletion of the vWF gene, which can cause severe vWD symptoms [13,14]. In conclusion, the development of vascular hemophilia is closely associated with mutations in the vWF gene.

vWF is a polysaccharide protein with molecular weight of 220kDa and secreted by endothelial cells and megakaryocytes. The mature vWF protein consists of 2050 amino acid residues including four major structural domains: D'-D3-A1-A2-A3-D4-C1-C2-C3-C4-C5-C6-CK, which interact with a wide range of molecules and cell types, forming multimers through disulfide bonding head-to-tail and molecular weights of up to several million Daltons [15–17]. This multimerization property is critical to the functionality of vWF as it increases binding to platelets and collagen [18,19]. At vascular injuries, vWF binds to exposed collagen through its A3 structural domain and promotes platelet adhesion by binding to the glycoprotein GPIb-IX complex on the platelet surface through the A1 domain; vWF also acts as a carrier for factor VIII, together ensuring that hemostasis and thrombosis occur at the appropriate time [20–22]. vWF's A2 structural domain is able to bind to ADAMTS13, a metalloproteinase, leading to the cleavage of vWF, thereby regulating vWF size and activity [15,23,24].

In normal circulation, vWF exists in a globular structure and does not bind to platelets. However, when the vasculature is damaged, exposed collagen and the local high shear environment induce a conformational change in vWF that exposes sites for binding to the platelet membrane GPIb-IX complex, forming a platelet-vWF-collagen complex. This process is particularly significant under high shear conditions, as shear enhances the binding of vWF to collagen[25–28]. Additionally, in a high shear environment, larger vWF multimers unfold more readily, exposing more binding sites and thus enhancing their ability to promote platelet adhesion and aggregation [29,30].

The effects of fluid shear on physiological function are widely used in a variety of fields including vascular health, bone development, cell biology and epithelial cell research. In physiology, fluid shear stress (FSS), which is a frictional force generated by blood, lymph, or other biological fluids on the walls of tubes or cell surfaces, is crucial in several physiological processes, ranging from vascular health, bone development to the biological function of epithelial cells [31–33]. Understanding and mastering these basic laws and mechanisms is not only important for basic science research, but also provides a theory and practical direction for the development and optimization of clinical treatment strategies.

As a large multimer, vWF is able to sense changes in shear forces in blood flow and plug ruptures in the vessel. The mechanisms behind this mechanosensing process are complex to study by conventional methods. Study with single-molecule imaging and high-pressure, fast-switching microfluidics revealed electrostatic guidance in speeding flow-activated vWF binding to GPIbα and recruiting platelets under flow conditions[34]. Single-molecule force measurements by atomic force microscopy (AFM) demonstrated strong interaction within vWF dimers, which dissociates at forces above 50 pN and provides ~80 nm of dimer elongation[35]. In type 2B von Willebrand disease, the mutations in A1 domain resulted in vWF inappropriate binding to platelet GPIBα with elongated bond lifetimes[36]. The intramolecular A1/A2 binding has auto-inhibitory effect on vWF recruiting platelets under normal circulation condition, which can be unfolded by shear force[37,38].

The *in vitro* study showed that multimerized vWF through sequential stacking steps is assembled as right-hand helical tubular storage, and clinical mutations of vWF in disrupting the assembly may lead to von Willebrand Disease[39]. The molecular length of vWF is regulated by shear-induced A2 domain unfolding, of which crystal structure shows a functional adaptation as a shear sensor[40]. Specifically, the usual structure of A domains in vWF contains the hydrophobic six

 doi:10.20944/preprints202502.0915.v1

β-strands encircled by six α-helices, while for A2 domain, the α4-helix is replaced by a loose loop, poor packing around the central β4-strand [40]. This feature in A2 structure may narrow the range of forces at which unfolding occurs, or they may slow the rate of refolding. The structure reveals von Willebrand disease mutations that are hypothesized to reduce the force of A2 unfolding.

It has been well recognized that the plastic vWF mechanosenses the hydrodynamic force to induce conformation change and elongated unfolding, which exerts its coagulation function to form complex with collagen and platelets. The previous studies visualized the elongation of vWF molecules under high shear forces, such as hundreds of dyn/cm^2 [37,41,42]. In this work, we applied Förster (fluorescence) resonance energy transfer (FRET) technology to study the conformation change of vWF in response to shear force. FRET has high sensitivity in measuring the subtle spatial changes within the molecules[43,44], which provided a suitable way to visualize the mechanosensation of vWF at physiological shear condition. By anchoring the vWF-based FRET biosensor on the surface of cell plasma membrane, our work revealed the high mechanosensation of vWF with two-level unfolding in responding to shear force, in which a flexible A2 domain and the large-molecular size of vWF are important contributing factors.

2. Materials and Methods

2.1. Cell Types and Sources

Human Embryonic Kidney Cells (HEK293T) are epithelial cells derived from human embryonic kidneys, purchased from BeiNa Biologics. The cells grow faster with enhanced adhesiveness and are modified to contain SV40 antigen, which enables them to express certain types of vectors and genes more efficiently, and are widely used in transfection experiments with high transfection efficiency[45]. The 293T cells were used to present the vWF-based biosensor on the cell surface to experience the flow experiments in this work.

2.2. Main Reagents and Instruments

High-glucose DMEM medium, fetal bovine serum (FBS), Opti-MEM medium, 0.25% trypsin-EDTA, cell detachment digestion reagent Accutase, and transfection kit Lipofectamine 3000 were purchased from Themo Fisher Scientific. The human full-length vWF in pcDNA3.1 vector was ordered from Addgene[46]. Hank's balanced salt solution (HBSS) was from Procell, Wuhan, China; single-channel flow chamber slides were from ibidi, Germany, and flow rate peristaltic pumps from Shanghai Feigeweit Company. FRET microscopy system and inverted microscope Primo Vert were purchased from Zeiss, Germany.

2.3. Constructions of vWF-Based FRET Biosensor and Related Mutant Plasmids

In the first step, the target fragment of A2 domain (Pro^{1490}-Cys^{1670}) from human full-length vWF, of which N-terminal contains 7 amino acid residues before β1-Strand as the flexible linker to ECFP, was amplified by PCR using pCS-CG-WT-Cer-vWF as the template[46]; the linear vector fragment of pcDNA3.1-ECFP-YPet without Camodulin-M13 part was obtained by PCR using pcDNA3.1-Ca^{2+}-YPet biosensor as the template[43]. The two linear fragments were ligated by Gibson Assembly kit (NEB) to obtain plasmid pcDNA3.1-ECFP-A2-YPet. The primers used in this step were designed according to the sequences of the ligated genes, and A2 domain amplification used the PCR primers as forward primer 1 (FP1): ttc gtg acc gcc gcc CCC AAG AGG AAC TCC, reverse primer 1 (RP1): ttc acc ttt aga cat ACC GGT ACA ACA ACT; the linear pcDNA3.1-ECFP-YPet fragment amplification by using FP2: AGT TGT TGT ACC GGT atg tct aaa ggt gaa gaa tta ttc act ggt; RP2: GGA GTT CCT CTT GGG ggc ggc ggt cac gaa ctc cag (letters in capital refers to the annealing part on the template DNA).

In the second step, ECFP-A2-YPet fragment was amplified by PCR using pcDNA3.1-ECFP-A2-YPet as the template; at the same time, pcDNA3.1-WT-vWF was used as the template for PCR to obtain the linear fragment pcDNA3.1-vWF-ΔA2 (without A2 domain). The two fragments were ligated by using Gibson Assembly kit, and then the plasmid pcDNA3.1-vWF-ECFP-A2-YPet were obtained by replacing A2 domain in vWF with ECFP-A2-YPet. The primers used in the second step as follows: ECFP-A2-YPet amplification with FP3: TTG GGG GTT TCG ACC CTG GGG atg gtg agc ggc gag gag, RP3: GGT GGG GAT CTG CAG CCC CTC ttt gta caa ttc att cat acc caa ttc att cat acc ctc ggt aat acc; pcDNA3.1-vWF-ΔA2 amplification with FP4: GGT ATT ACC GAG GGT ATG AAT GAA

 doi:10.20944/preprints202502.0915.v1

TTG tac aaa gag ggg ctg cag atc ccc acc, RP4: CTC CTC GCC CTT GCT CAC CAT ccc cag ggt cga aac ccc caa.

In the third step, the achieved plasmid pcDNA3.1-vWF-ECFP-A2-YPet was further swapped into the vector pDisplay which can present the expressed biosensor protein on the cell membrane surface. This subcloning step was done by a commercial company Beijing BGI Genomics Co. to acquire the plasmid pDisplay-vWF-ECFP-A2-YPet along with sequencing confirmation. Then, pDisplay-vWF-ECFP-LOCK-A2-YPet version was generated by the company through mutation of Asp^{1493} and Cys^{1669} to Cys^{1493} and Gly^{1669} at the N and C-terminal of A2 domain, respectively. Hence, the mutated A2 structural domain forms double-sulfide bond between its N and C- terminals to prevent the proper confirmation change, named as LOCK-A2[46]. Specifically, the A2 sequence at N-terminal CCC AAG AGG AAC TCC and C-terminal AGT TGT TGT ACC GGT were changed to CCC AAG AGG TGC TCC and AGT GGT TGT ACC GGT. The short versions of ECFP-A2-YPet only and ECFP-LOCK-A2-YPet only FRET biosensors were constructed into pDisplay vector as derived from their full-length vWF FRET biosensors by BGI Genomics Co.

All the mentioned plasmids used in this work are ampicillin (Amp) resistant, and were amplified by Midi plasmid extraction kit (QIAGEN). The DNA concentrations were measured by NanoDrop (TECAN), and the plasmids could be used in a series of subsequent cell transfection experiments.

2.4. 293T Cell Culture and Transfection with FRET Biosensors

293T cells were cultured in high-glucose DMEM (Dulbecco's Modified Eagle Medium) medium supplemented with 10% FBS and double-antibiotics, and placed in a 37°C humidified incubator containing 5% CO2. The cells used in the experiments were generally passaged no more than 10 times. According to the transfection method of Lipofectamine 3000 liposomes (Thermo Invitrogen), cells were inoculated into 24-well plates in normal culture medium without antibiotics one day before transfection, and the cell density reached 60%~80% at the time of transfection. Each well was transfected with 1 μg plasmid DNA; after 8~12 h, the medium was replaced with fresh medium without antibiotics. After 24 h from the start of transfection, cells were digested with Accutase solution, and transferred into ibidi newly unsealed or fully sterilized single-channel slides (μ-Slide $I^{0.4}$ Luer, 5 mm x 50 mm in channel width and length) and replaced with fresh culture medium containing 1% FBS. The experiments of cell flow microscopy imaging were started two days after the transfection.

2.5. Fluid Shear Experimental Setup and FRET Microscope Imaging

Before the start of the experiment, a suitable hose (Size-$14^{\#}$) was connected to the single-channel flow chamber slide (μ-Slide $I^{0.4}$ Luer) through a Luer fitting, and then the hose was connected to a peristaltic pump. The inlet and outlet ports were inserted into a centrifuge tube prepared with 20 ml of HBSS solution, and the tube was placed in a tube rack. It should be noted that before starting the fluid experiment, the HBSS solution in the inlet port should be pumped to the Luer connector using a peristaltic pump to ensure that the single-channel flow chamber slide was filled with the liquid and seamlessly connected to each other. This prevented air bubbles from being generated during the flow of the liquid, hence not affecting the stability of the experiment.

According to the protocol from the manufacturer ibidi, shear force calculation for μ-Slide $I^{0.4}$ Luer is as follows: $\tau = \eta \cdot 131.6 \cdot \Phi$, of which Φ: flow rate mL/min, τ: shear stress in dyn/cm², and η: dynamical viscosity in dyn·s/cm². η = 0.00106 dyn·s/cm² for HBSS measured by Malvern Kinexus rheometer at room temperature.

In the FRET microscope system, the filter parameters were excitation (436±10) nm, dichroic mirror 455 nm for both ECFP and FRET channels, emission (475±20) nm and emission (535±15) nm for ECFP and FRET (YPet) channel, respectively. In the imaging experiments, we used an ×100 oil objective to take the FRET images. The fast switching of ECFP and FRET imaging channels was controlled by Zeiss software system to ensure the simultaneous acquisition of image data from both channels. During the experimental flow process, fluorescence images were collected at 2-minute interval, and the peristaltic pump, which had been set in advance to correspond to the experimental parameters, was turned on after 10 minutes of FRET imaging, and the total flow administrating time was 30 minutes. The images were acquired at room temperature, due to lacking of an appropriate temperature controller to fit the fluidic system in the lab yet.

 doi:10.20944/preprints202502.0915.v1

2.6. Quantitative and Statistical Analysis of FRET Image Data

The FRET signals from the experimental image raw data were quantified by FRET image analysis software FluoCell 6.0.0[47]. The ratios of fluorescence intensity between ECFP and FRET channels were calibrated pixel to pixel after subtracting background effects, and the ratiometric images as well as FRET/ECFP ratio data were acquired. Statistical analysis of the data was carried out in GraphPad Prism 6.0 software. Time-course curves and plots with scattering points (mean ± S.E.M.) of FRET ratios were analyzed, as well as the differences between each of the two data sets.

Differences between data sets were analyzed using one-way ANOVA test between the control and experimental groups, and one pair analysis was performed by Student's t-test. *, **, ***, **** represent p-values <0.05, 0.01, 0.001, and 0.0001 for significant differences, while "ns" indicates no significant difference.

3. Results

3.1. Design of vWF-Based FRET Biosensor and Flow Experimental Setup

vWF is a large-size protein made by endothelial cells/megakaryocytes to store in Weibel–Palade bodies or stay in the circulation system[48]. vWF can sense the hydrodynamic force at the injured site of the vascular vessels, which helps unfold the protein to recruit platelets in assembling clots and stopping the bleeding[38,49]. A2 domain in vWF has been identified as one mechanosensing element during the thrombus formation[46]. Researches from *in vitro* models visualized the elongated vWF molecules under high shear flow, such as hundreds of dynes per cm^2[37,41,42]. In this work, we applied FRET responses to study vWF in sensing the hydrodynamic force, which research tool has high sensitivity in monitoring the molecular conformation.

The FRET pair of fluorescent proteins ECFP and YPet were inserted into the full-length vWF, as the A2 domain was flanked by the FRET pair (shown in Figure 1A). The vWF-based FRET biosensor was subcloned into pDisplay vector which could direct the protein to the secretory pathway and anchor the biosensor on the surface of cell plasma membrane by the transmembrane domain from platelet-derived growth factor receptor (PDGFR)[50]. This positioning scenario helped mimic vWF sensing the hydrodynamic force while sticking to the under-endothelial layer of vascular wall. We also prepared the mutated version by forming a disulfide bond between A2's N and C-termini (LOCK-A2), named as LOCK-vWF biosensor (Figure 1B). The LOCK-A2 could resist the conformation change for vWF self-associations induced by flow shear[46].

In the fluidic and FRET microscopy setup (Figure 1C), 293T cells were seeded into the single-channel fluidic slide after transfection of the biosensor for 24 h, and maintained in culture medium with 1% FBS (low serum to reduce the shedding possibility of the biosensor on the cell surface). HBSS solution was applied for the flow, which can maintain the cell condition for hours long. The peristaltic pump was able to adjust the flow force through the chamber slide (μ-Slide $I^{0.4}$ Luer) from 0.0027 to 178.1 mL/min within ±0.5% variation in accuracy. The FRET imaging was conducted at room temperature, and the imaging process was generally completed in 40 min.

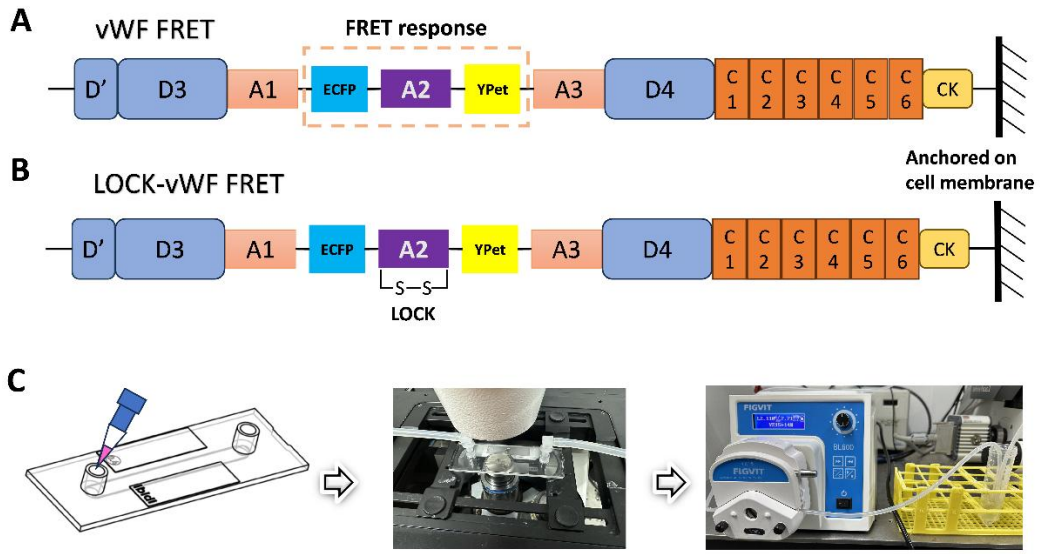

 doi:10.20944/preprints202502.0915.v1

Figure 1. Design of vWF-based biosensor and flow experimental setup. **(A, B)** Schematic diagrams of the vWF or LOCK-vWF-based FRET biosensor. A2 domain is flanked by ECFP and YPet, and the biosensor protein is anchored on the surface of cell plasma membrane. **(C)** The setup of flow experiments on the microscope. The image of microfluidic chamber was adapted from the manufacturer ibidi.

3.2. Changes of vWF-Based FRET in Response to Different Shear Forces

To examine whether the vWF-based biosensor was able to detect the hydrodynamic force, we applied different magnitudes of shear stress from 0 to 28 dyn/cm² to the cells seeding in the microfluidic channels. 293T cells expressing the vWF-based biosensor on the cell surface showed apparent FRET responses to the shear flow, as presented by the FRET ratiometric images in Figure 2A (Movie 1). Specifically, for the cells implanted on the single-channel flow chamber slides, when without applying shear force to the cells, the FRET values did not change significantly (0 dyn); when the peristaltic pump was turned on to apply shear force, the biosensor showed clear FRET changes with the ratio (FRET/ECFP) increasing along the time. The cells generally had more FRET changes at the cell boundaries, in corresponding to shear force exerting on the cell surface. The time-course curves from FRET/ECFP ratio quantifications on the cells demonstrated no FRET changes before flow, and gradual increases after flow applications (Figure 2B).

To compare the FRET changes under different magnitudes of shear forces, 2.8 dyn/cm² induced more changes (60%) than 1.4 dyn/cm² (38%) in 30 min (Figure 2C). The FRET changes didn't continue to increase under higher flow magnitudes, instead after reached the peak at 2.8 dyn/cm², the FRET change rate started to decrease from 2.8 to 28 dyn/cm² (Figure 2C). Based on the FRET efficiency calibrations, these results indicate that the two terminals of A2 domain in vWF were getting closer spatially under low shear force (0-2.8 dyn/cm²), and then becoming more separated at higher shear (2.8-28 dyn/cm²). The observations from FRET measurements seemed to point to unfolding of vWF at two stages: at low shear force, A2 dissociated from vWF intramolecular binding such as A1/A3 domains, and then under higher shear force, A2 domain was unfolded for cleavage accessing by ADAMTS13. The underlying mechanism requires further investigation.

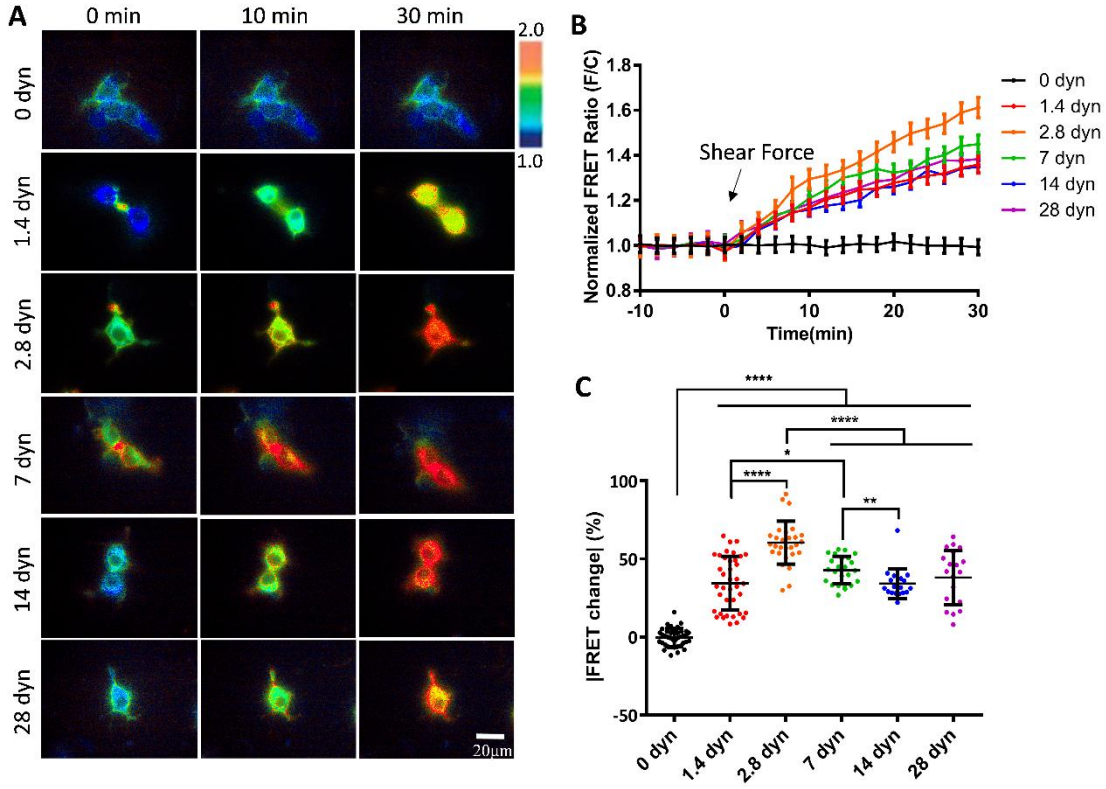

Figure 2. FRET changes of vWF-based biosensor in 293T cells under gradient flow shears. (A) FRET ratiometric images of cells expressing vWF-based biosensor at 0, 10 and 30 min under fluid shear of 0, 1.4, 2.8, 7, 14, 28 dyn/cm², with 0 dyn as control. **(B)** The time-course curves of FRET ratio (FRET/ECFP) quantifications

 doi:10.20944/preprints202502.0915.v1

(mean ± S.E.M.) for the cell groups in (A) under the indicated shear forces. **(C)** Scatter plots of quantified FRET ratio changes for vWF-based biosensor at 30 min under indicated shear forces. The experiment was repeated three times independently. The specific values (mean ± S.E.M.) in (C): 0 dyn, -0.32 ± 0.90, N=40; 1.4 dyn, 34.41 ± 2.80, N=38; 2.8 dyn, 60.49 ± 2.55, N=29; 7 dyn, 42.77 ± 1.81, N=24; 14 dyn, 34.14 ± 2.20, N=19; 28 dyn, 38.04 ± 3.89, N=20. N refers to the sample size. *, **, ***, **** indicate P < 0.05, 0.01, 0.001, and 0.0001 by one-way ANORA test; 'ns' denotes non-significant difference, and so on through this paper.

3.3. Sensitive FRET Responses of the vWF-Based Biosensor to Micro-Shear Flow

We further examined the mechanosensitivity of vWF under the scale of micro-shear forces. A gradual increment of micro-shear forces ranging from 0.14 to 1.4 dyn/cm² was chosen to study the sensitivity of vWF-based FRET responses. The results showed that these micro-shear forces were sufficient to induce FRET responses from the conformation changes of vWF-based biosensor (Figure 3A). Specifically, the FRET changes were positively correlated with the magnitudes of the micro-shear forces (0.14-1.4 dyn/cm²) (Figure 3B), demonstrating the ability of cell membrane-anchored vWF-based biosensor in sensing the tiny hydrodynamic forces. By quantitatively comparing the responses to the gradient micro-shear forces, the FRET changes showed difference as early as 6 min after the flow applications with the lowest response from 0.14 dyn/cm², while 1.4 dyn/cm² had the relatively higher response than the others through the 30 min flow processes (Figure 3C). These data indicate that the membrane-anchored vWF molecules are highly sensitive to the hydrodynamic forces.

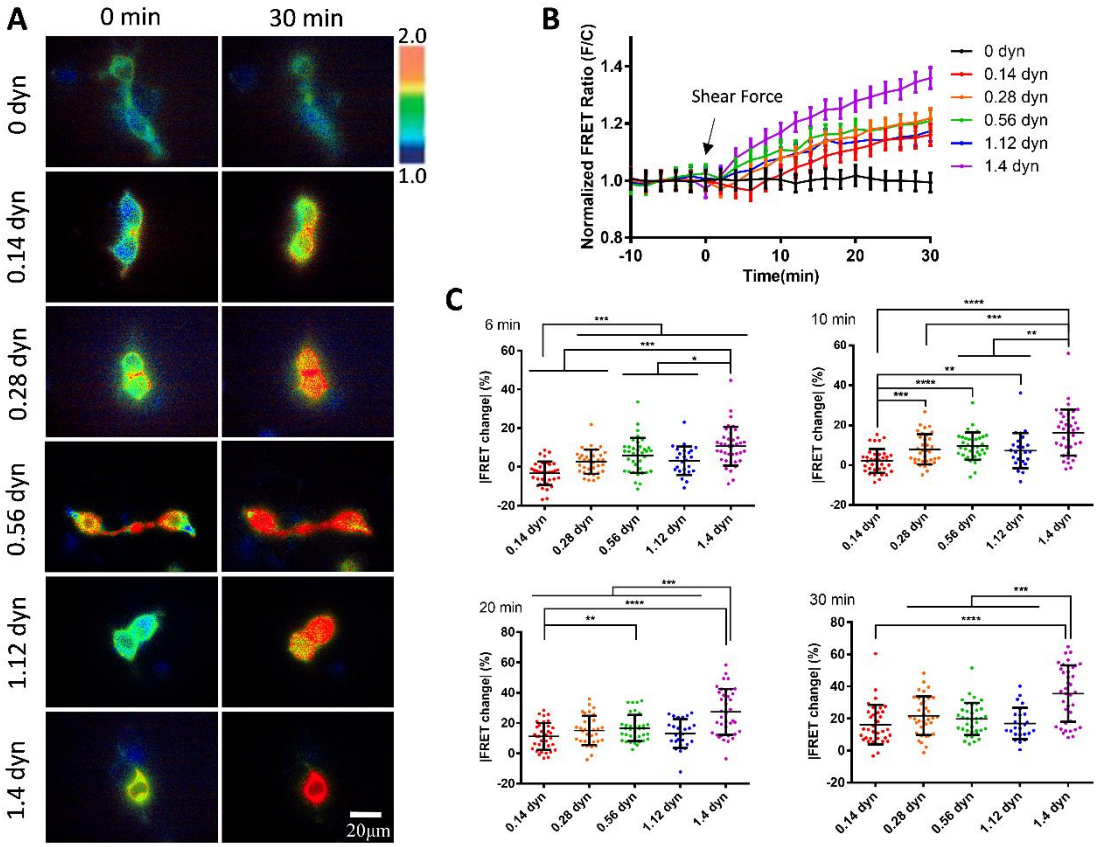

Figure 3. vWF-based FRET responses under micro-shear forces from 0.14-1.4 dyn/cm². (A) Representative ratiometric FRET images of 293T cells expressing vWF-based biosensor at 0 and 30 min after applying 0, 0.14, 0.28, 0.56, 1.12, 1.4 dyn/cm² micro-shear flow. **(B)** The time-course curves of normalized FRET changes (mean ± S.E.M.) before and after the micro-shear flow (0.14-1.4 dyn/cm²), with 0 dyn/cm² as control. **(C)** Statistical comparisons of FRET changes in percentages (mean ± S.E.M.) after applications of the different micro-shear flows (0.14-1.4 dyn/cm²) at 6, 10, 20, 30 min, respectively. The percentage values (mean ± S.E.M) at 30 min as follows: 0.14 dyn, 16.16±2.06, N=36; 0.28 dyn, 21.71±2.04, N=35; 0.56 dyn, 19.68±1.65, N=37; 1.12 dyn, 16.90±1.95, N=25; 1.4 dyn, 35.48±2.86, N=38. N refers to the sample size. The experiment had three independent repeats.

3.4. Shear Force-Induced vWF FRET Response from A2 Conformation Change

 doi:10.20944/preprints202502.0915.v1

To further investigate the molecular mechanism of shear force-induced vWF FRET response, we constructed a A2-LOCK version of vWF biosensor in which the N and C-termini of A2 domain were linked by a disulfide bond (Figure 1B). Our recent work also demonstrated the advantage of FRET application in verifying intermolecular interaction sites[51]. The previous study showed that the vWF mutant with LOCK-A2 exhibited attenuated vWF self-associations, collagen and platelets bindings, and ADMAMTS13 cleavage under shear flow[46]. To check whether the flow-induced FRET change was vWF-dependent, we included MT1-MMP biosensor as control which is also located in pDisplay vector and presented on the cell surface as a non-plastic and small-size protein[50].

The flow at 2.8 dyn/cm² induced about 60% FRET change of vWF-based biosensor in 30 min, but little FRET changes for LOCK-vWF or MT1-MMP biosensor (Figure 4A-C. Movie 2). This indicates that the hydrodynamic force-induced FRET response depended on the specific feature of vWF molecules. LOCK-A2 domain in vWF biosensor could resist the flow-induced conformational change, suggesting that the A2 unfolding was important for vWF sensing of the hydrodynamic force. MT1-MMP biosensor showed little FRET response, which confirmed the FRET change in vWF not due to shear force on the FRET pair, and also suggested the large molecular size or plastic feature of vWF crucial in the flow mechanosensation.

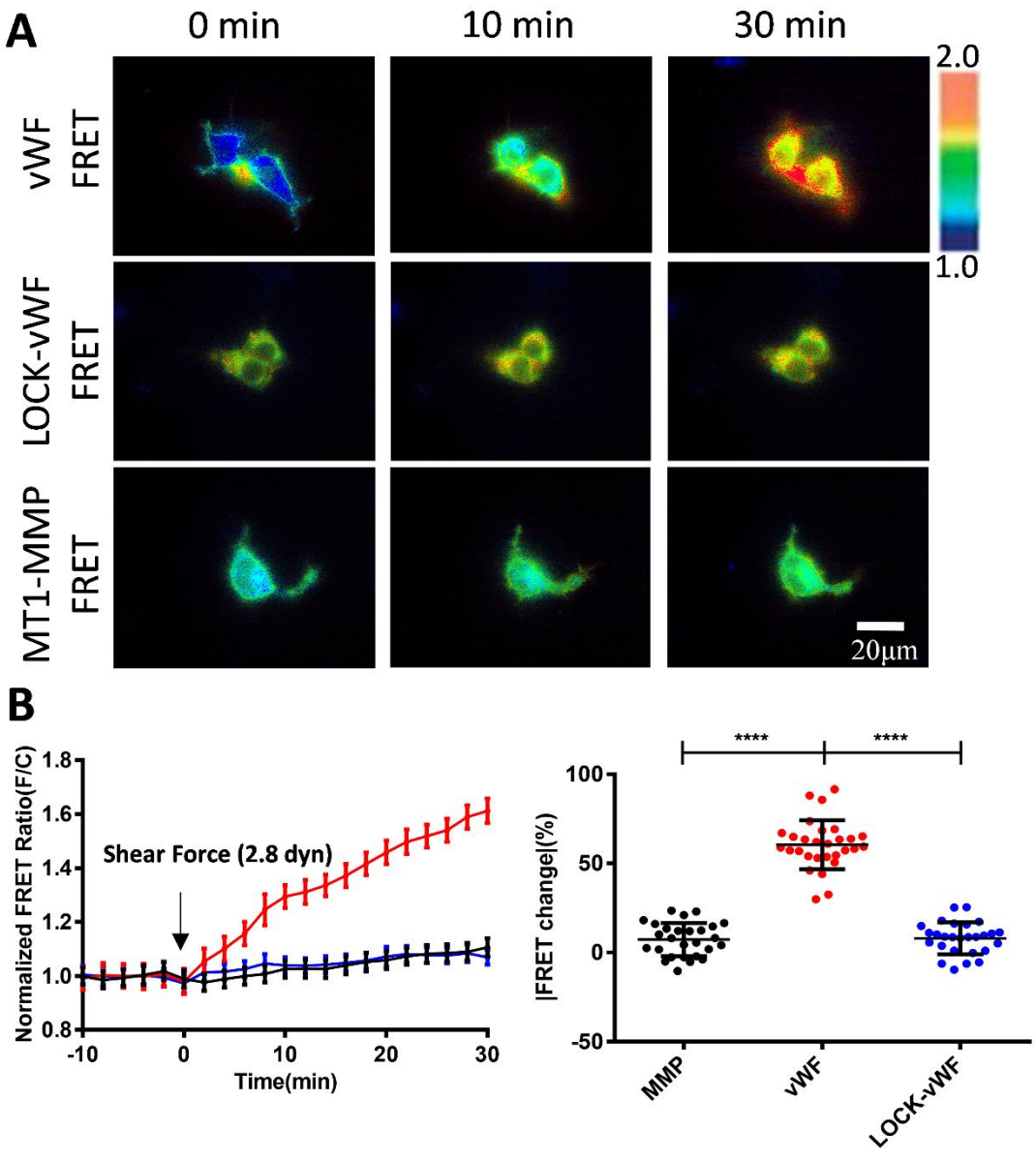

Figure 4. Comparisons for flow-induced FRET responses of vWF and LOCK-vWF-based biosensors as well as small-size MT1-MMP biosensor. (A) Representative ratiometric FRET images of 293T cells expressing vWF or LOCK-vWF-bazsed biosensor, or MT1-MMP biosensor in response to 2.8 dyn/cm² shear force. (B) The time-

 doi:10.20944/preprints202502.0915.v1

course curves (left) and scatter plots (at 30 min, right) of quantified FRET changes for the cell groups in (A). The values of scatter plots (mean±S.E.M.) are listed here: vWF-FRET, 60.49±2.56, N=29; LOCK-vWF-FRET, 7.36±1.81, N=27; MT1-MMP FRET, 8.08±1.73, N=27. N refers to the sample size.

3.5. Response of A2 Only-Based FRET Biosensor to the Hydrodynamic Force

A2 domain is the mechanosensitive element in vWF responding to the hydrodynamic force. Hence, we constructed A2-based FRET biosensor to investigate whether A2 domain only was able to sense the low magnitude flow, or depended on the large size of vWF molecules. The expressed A2 biosensor and LOCK-A2 biosensor were anchored on the surface of cell plasma membrane (Figure 5A). Under 2.8 dyn/cm^2 shear force on the seeded cells in the fluidic channel, vWF-based biosensor showed apparent FRET response with ~60% change in 30 min, whereas A2 FRET or LOCK-A2 FRET biosensor didn't have obvious FRET response (Figure 5B-D, Movie 3). It is noticed that A2 only biosensor had a much higher FRET basal level (FRET/ECFP ratio: ~2.0) than that of vWF-based biosensor (ratio: ~1.3) (Figure 5C), which suggests a closer positioning of the N and C-terminals in A2 only, or that vWF had a pulling force on A2 domain in the full-length molecules. We further applied higher shear force (14 dyn/cm^2) on the three versions of biosensors, which didn't activate A2 only-based biosensor, either (Figure 5E&F). Hence, at the low-scale flow rate (below 14 dyn/cm^2), the plastic vWF with large molecular size seems essential to sense the shear force and induce A2 unfolding.

 doi:10.20944/preprints202502.0915.v1

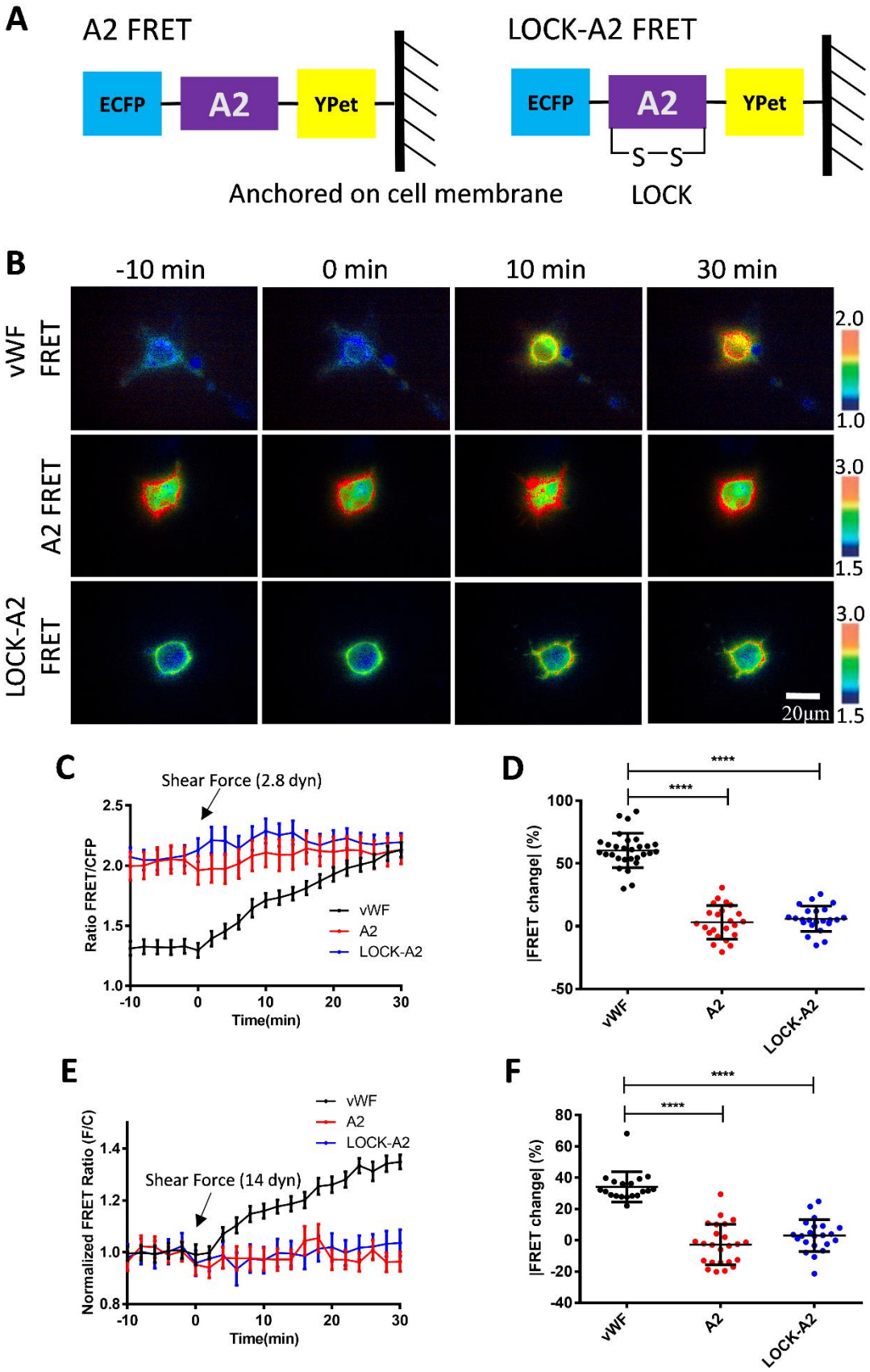

Figure 5. The response of A2-based FRET biosensor to shear force. (A) The design of FRET biosensors based on A2 only and LOCK-A2, and anchored on the surface of cell plasma membrane. **(B)** Representative ratiometric FRET images of 293T cells expressing vWF FRET, A2 FRET, or LOCK-A2 FRET biosensor in response to 2.8 dyn/cm² shear force. **(C, D)** The time-course curves (C) and scatter plots (at 30 min, D) of FRET changes for the cell groups under 2.8 dyn/cm² condition (B). The percentage values of scatter plots (mean±S.E.M) as follows: vWF, 60.49±2.55, N=29; A2 only, 3.13±2.76, N=23; LOCK-A2 only, 5.92±2.09, N=23. **(E, F)** The time-course curves

 doi:10.20944/preprints202502.0915.v1

(E) and scatter plots (at 30 min, F) of FRET change quantifications for the indicated cell groups in response to 14 dyn/cm^2. The percentage values of scatter plots in (F) (mean±S.E.M): vWF, 34.14±2.20, N=19; A2 only, -2.77±2.66, N=24; LOCK-A2 only, 3.01±2.19, N=22. N refers to the sample size. The experiments were repeated 3 times, independently.

4. Discussion

vWF has been recognized as a biomechanical probe in assisting the hydrodynamic force-induced coagulation and thrombus formation at the wound of vascular injury. Recent work provided the probable insight that the initial vWF-binding collagen at the injured subendothelial layer may be independent of flow force, while the following binding of platelets relies on the shear-induced unfolding of vWF[52]. This hypothesis may help explain that free vWF isn't sensitive to the regular flow in the circulation system, but anchored vWF at the injured sites becomes unfolded by shear force, therefore to further recruit platelets in assembling the clots. A2 domain is established as a mechanosensitive element in vWF to promote conformation change and elongation of this molecule in response to shear force[40,46]. In this work, we constructed a FRET-based biosensor anchored on the cell surface to monitor the vWF mechano-response to the hydrodynamic force, in which design the A2 domain is flanked by ECFP and YPet pair (Figure 1A-C). As a technology, FRET efficiency is highly sensitive to the spatial change between the pair, as inversely proportional to the sixth power of the distance[53], which can provide an untraditional way to monitor the shear-induced conformation change of vWF molecules.

We applied microfluidic channels to study the shear response of vWF-based FRET biosensor presenting on the cell surface. Fluid shear is closely related to the developmental processes and physiological activities, and has important impacts on a variety of cardiovascular and hematologic diseases. How shear stress is involved in regulating the function of vWF proteins has been a hot topic in research. The results from our FRET measurements showed significant response of the biosensor to the hydrodynamic force, with 60% FRET change at 2.8 dyn/cm^2 in 30 min, which is higher than the 38% change at 1.4 dyn/cm^2, but the FRET response didn't continue increase with further enhanced flow from 7-28 dyn/cm^2 (Figure 2A-C). When applied gradient micro-shear flow below1.4 dyn/cm^2, the FRET response was still obvious at 0.14 dyn/cm^2, and displayed certain gradual changes from 0.14-1.4 dyn/cm^2 (Figure 3A-C). These FRET measurements indicate the high sensitivity of vWF in responding to shear force even under 1.4 dyn/cm^2, which seems consistent with the clot formation at the minor skin wounds. In comparison to the previous visualizations of vWF elongation under high flow rate (hundreds of dyn/cm^2), this FRET-based study of vWF unfolding was able to sensitively monitor the vWF conformation change under low shear force (several dyn/cm^2).

As mentioned in the Results, the flow induced increase of FRET efficiency between ECFP and YPet (Figs. 2&3), indicating a closer positioning of N and C-terminals of A2 domain. This measured result seems contradictive to the predicted unfolding of A2 domain in vWF by high shear force. Hypothetically from a different angle, in considering that A2 domain binds to A1 domain or plus A3 as an intramolecular autoinhibitory mechanism for vWF[38,54,55], the flow induced dissociation of A2 from A1 binding during vWF unfolding, which resulted in closer positioning of the N and C-terminals of A2 domain. In supporting this, the A2 only biosensor showed much higher FRET level than that of vWF-based biosensor (Figure 5C), indicating closer positioning of the two termini of released A2 domain without A1 or A3 binding.

It is interesting to notice that the micro-flow induced a gradual increase of the FRET efficiency at low shear scale of 0-2.8 dyn/cm^2, which then started to decline from 2.8-28 dyn/cm^2 (Figure 2C). The observations from FRET measurements seemed to point to two-level unfolding of vWF: A2 dissociation from vWF intramolecular binding of A1/A3 domains at low shear force, and then unfolding of A2 domain under higher shear force for cleavage accessing by ADAMTS13. This conclusion drawn from FRET measurement may not be a surprise from studying previous literatures. First, the mutual interaction of A-domains in vWF has been demonstrated experimentally[56], and application of stretching force at ~20 pN by optical trap elongated the engineered protein fragment consisting of three repeats of (A1-A2-A3) domains[57]. Second, single-molecular experiments with laser tweezers proved mechanoenzymatic cleavage of A2 in vWF by ADAMTS13, in which only stretch-unfolded A2 domain is accessible to the enzymatic cleavage[58]; LOCK-A2 domain that prevents A2 unfolding reduced vWF self-association and binding of platelets under flow shear[46]. Third, single-molecular stretch did show two unfolding events or extension peaks of vWF,

 doi:10.20944/preprints202502.0915.v1

specifically at the pulling forces of ~23 pN and ~40 pN[57]. Although the previous work didn't distinguish the intramolecular dissociation of A-domains in vWF from A2 unfolding, our FRET measurements from the designed vWF biosensor could help reveal the two-level unfolding of vWF by the spatial intramolecular conformation changes.

Previous studies have shown that the cause of some vascular hemophilia is due to the inability of the A2 structural domain in vWF to undergo a conformational change in the patient as compared to the normal human. A2 domain is the mechanosensitive element in vWF, and LOCK-A2 domain (with a disulfide-bond bridging of its N and C-terminals) could resist the shear flow-induced vWF self-association and ADAMTS13 cleavage[46]. We generated a version of vWF-based FRET biosensor containing LOCK-A2 (LOCK-vWF FRET), and also introduced a MT1-MMP biosensor as control which is located on the cell surface but with small molecular size[50]. Under 2.8 dyn/cm^2 flow, vWF FRET showed 60% FRET change in 30 min, while LOCK-vWF (with higher basal FRET ratio) or MT1-MMP biosensor had very little FRET change (Figure 4A&B). These results demonstrated that structure-flexible A2 domain is essential for the flow-induced conformation change, and confirmed that the observed FRET change of vWF biosensor was not from shear force exerting on the ECFP/YPet pair.

We further constructed A2 only FRET biosensor and its LOCK-A2 version, which didn't show obvious FRET responses to 2.8 and 14 dyn/cm^2 (Figure 5A-F). An earlier study reported that chemical denaturation of A2 domain by 6 M Urea caused unfolding of A2 domain and decrease in FRET efficiency of A2-based biosensor[59]. Our data indicates that A2 only isn't sensitive to the hydrodynamic force (14 dyn/cm^2), and the integrity of full-length vWF reserves the ability of high mechano-sensitivity to shear force even at low scale as 0.14 dyn/cm^2. It is noted that A2 only biosensor had much higher FRET level (ratio: ~2.0) than that of vWF-based biosensor (ratio: ~1.3) (Figure 5C). This seems consistent with the shear-induced FRET increase of vWF biosensor, which may be resulted from shear-induced dissociation of A2 domain from binding of A1 and A3 domains.

In summary, we developed a shear force biosensor based on the mechanosensitive nature of vWF molecules. By combining FRET imaging with microfluidic channel, the biosensor anchored on the cell surface displayed high sensitivity to the hydrodynamic force with increasing FRET responses along with micro-shears from 0.14 to 2.8 dyn/cm^2, which started to decline at higher magnitude 2.8-28 dyn/cm^2. The gradient shear-induced increase and then decease in FRET efficiency indicates two-level unfolding of vWF: the dissociation of A2 domain from vWF intramolecular binding under low shear, which is supported with stronger FRET of A2 only-based biosensor, and then unfolding of A2 domain in vWF under higher shear, which is consistent with previous work (illustrated in cartoon Figure 6). The LOCK-vWF biosensor lost FRET response to the hydrodynamic force, indicating a structure-flexible A2 important for the force mechanosensation. The FRET biosensor containing A2 only couldn't respond to the shear force under 14 dyn/cm^2, implying that the large vWF molecule is needed for the normal physiological functions during shear-induced coagulation and thrombus assembly. Besides the previous biomechanical studies of vWF, the FRET technology shows high sensitivity and experimental convenience in monitoring the conformation change of vWF molecules.

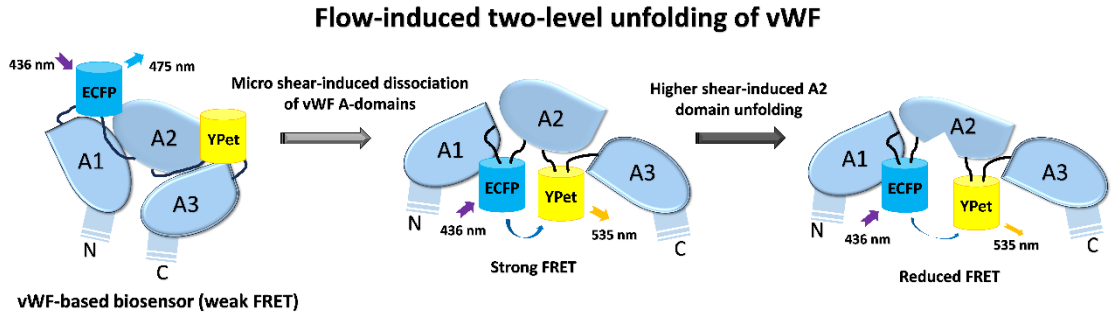

Figure 6. Illustrated model of shear-induced vWF unfolding. Based on the data from this work along with previous studies, shear flow induces two-level unfolding of vWF-based biosensor: the dissociation of A-domains in vWF molecules under low shear force, which results in an increase of FRET efficiency in the vWF-based biosensor; followed by the unfolding of A2 domain under higher shear force, which results in declining FRET efficiency.

 doi:10.20944/preprints202502.0915.v1

Further research is needed to clarify the underlying molecular mechanisms for shear-induced two-level unfolding of vWF. The *in vitro* study by purifying the vWF-based biosensor protein can help validate the vWF function in binding to collagen and platelets. The FRET imaging can also be moved to vascular cells as more physiologically relevant, or with higher flow rate. As additional factor, further input of ADAMTS13 enzyme in the flow may help understand its role in vWF mechanosensation and conformation change.

Author Contributions: M.O. and L.D. designed the experiments; Y.G. performed the majority of experiments and data analysis; B.Z. and Y.G. constructed the biosensor plasmids; Y.G. and M.O. carried the data organization; J.G. and L.L. had technical help; Y.W. provided conceptual advice and discussion; L.D. provided the setups of equipment; M.O., Y.G., Y.W. and L.D. prepared the manuscript.

Acknowledgments: We appreciate the helpful comments on this work from Professor Cheng Zhu and Amir Ashkezari (Georgia Institute of Technology). The human vWF plasmid from Addgene was deposited by Sriram Neelamegham Lab, State University of New York. The experiments were assisted by lab technicians Lei Liu, Yan Pan, and Jingjing Li (Changzhou University). This work was funded by National Natural Science Foundation of China (NSFC 12372312), and Project of "Jiangsu Specially-appointed Professor" (M.O.); National Natural Science Foundation of China (NSFC 12272063) (L.D.).

Conflict of Interest: The vWF-based FRET biosensor is under filing for a patent named as "von Willebrand Factor (vWF)-based FRET biosensor for detection of shear force and study of vWF mechanosensation". The authors declare no other conflicts of interest with the contents of this article.

References

1. Neff, A. T., and Sidonio, R. F. (2014) Management of VWD. *Hematol.-Am. Soc. Hematol. Educ. Program*, 536-541
2. Federici, A. B. (2014) Clinical and laboratory diagnosis of VWD. *Hematol.-Am. Soc. Hematol. Educ. Program*, 524-530
3. Abshire, T. C. (2006) Prophylaxis and von Willebrand's disease (vWD). *Thrombosis research* **118 Suppl 1**, S3-7
4. Flood, V. H. (2014) New insights into genotype and phenotype of VWD. *Hematology. American Society of Hematology. Education Program* **2014**, 531-535
5. DiGiandomenico, S., Christopherson, P. A., Haberichter, S. L., Abshire, T. C., Montgomery, R. R., and Flood, V. H. (2021) Laboratory variability in the diagnosis of type 2 VWD variants. *Journal of thrombosis and haemostasis : JTH* **19**, 131-138
6. Favaloro, E. J., and Pasalic, L. (2022) Laboratory Diagnosis of von Willebrand Disease (VWD): Geographical Perspectives. *Seminars in thrombosis and hemostasis* **48**, 750-766
7. James, P., Leebeek, F., Casari, C., and Lillicrap, D. (2024) Diagnosis and treatment of von Willebrand disease in 2024 and beyond. *Haemophilia : the official journal of the World Federation of Hemophilia* **30 Suppl 3**, 103-111
8. Lenting, P. J., Christophe, O. D., and Denis, C. V. (2015) von Willebrand factor biosynthesis, secretion, and clearance: connecting the far ends. *Blood* **125**, 2019-2028
9. Anderson, J. R., Li, J., Springer, T. A., and Brown, A. (2022) Structures of VWF tubules before and after concatemerization reveal a mechanism of disulfide bond exchange. *Blood* **140**, 1419-1430
10. Michiels, J. J., Berneman, Z., Gadisseur, A., van der Planken, M., Schroyens, W., van de Velde, A., and van Vliet, H. (2006) Characterization of recessive severe type 1 and 3 von Willebrand Disease (VWD), asymptomatic heterozygous carriers versus bloodgroup O-related von Willebrand factor deficiency, and dominant type 1 VWD. *Clinical and applied thrombosis/hemostasis : official journal of the International Academy of Clinical and Applied Thrombosis/Hemostasis* **12**, 277-295
11. Curnow, J., Pasalic, L., and Favaloro, E. J. (2016) Treatment of von Willebrand Disease. *Seminars in thrombosis and hemostasis* **42**, 133-146
12. Ewenstein, B. M. (1997) Von Willebrand's disease. *Annual review of medicine* **48**, 525-542
13. Veyradier, A., Boisseau, P., Fressinaud, E., Caron, C., Ternisien, C., Giraud, M., Zawadzki, C., Trossaert, M., Itzhar-Baïkian, N., Dreyfus, M., d'Oiron, R., Borel-Derlon, A., Susen, S., Bezieau, S., Denis, C. V., and Goudemand, J. (2016) A Laboratory Phenotype/Genotype Correlation of 1167 French Patients From 670 Families With von Willebrand Disease: A New Epidemiologic Picture. *Medicine* **95**, e3038

 doi:10.20944/preprints202502.0915.v1

14. de Jong, A., and Eikenboom, J. (2017) Von Willebrand disease mutation spectrum and associated mutation mechanisms. *Thrombosis research* **159**, 65-75
15. Favaloro, E. J., Henry, B. M., and Lippi, G. (2021) Increased VWF and Decreased ADAMTS-13 in COVID-19: Creating a Milieu for (Micro)Thrombosis. *Seminars in thrombosis and hemostasis* **47**, 400-418
16. Xiang, Y., and Hwa, J. (2016) Regulation of VWF expression, and secretion in health and disease. *Current opinion in hematology* **23**, 288-293
17. Favaloro, E. J. (2024) The Role of the von Willebrand Factor Collagen-Binding Assay (VWF:CB) in the Diagnosis and Treatment of von Willebrand Disease (VWD) and Way Beyond: A Comprehensive 36-Year History. *Seminars in thrombosis and hemostasis* **50**, 43-80
18. Howes, J. M., Knäuper, V., Malcor, J. D., and Farndale, R. W. (2020) Cleavage by MMP-13 renders VWF unable to bind to collagen but increases its platelet reactivity. *Journal of thrombosis and haemostasis : JTH* **18**, 942-954
19. Favaloro, E. J., and Mohammed, S. (2017) Laboratory Testing for von Willebrand Factor Collagen Binding (VWF:CB). *Methods in molecular biology (Clifton, N.J.)* **1646**, 417-433
20. Seidizadeh, O., and Peyvandi, F. (2023) Laboratory Testing for von Willebrand Factor Activity by a Glycoprotein Ib-Binding Assay (VWF:GPIbR): HemosIL von Willebrand Factor Ristocetin Cofactor Activity on ACL TOP(®). *Methods in molecular biology (Clifton, N.J.)* **2663**, 669-677
21. Eikenboom, J., Federici, A. B., Dirven, R. J., Castaman, G., Rodeghiero, F., Budde, U., Schneppenheim, R., Batlle, J., Canciani, M. T., Goudemand, J., Peake, I., and Goodeve, A. (2013) VWF propeptide and ratios between VWF, VWF propeptide, and FVIII in the characterization of type 1 von Willebrand disease. *Blood* **121**, 2336-2339
22. Kanaji, S., Fahs, S. A., Shi, Q., Haberichter, S. L., and Montgomery, R. R. (2012) Contribution of platelet vs. endothelial VWF to platelet adhesion and hemostasis. *Journal of thrombosis and haemostasis : JTH* **10**, 1646-1652
23. Jang, J., Gu, J., and Kim, H. K. (2022) Prognostic value of the ADAMTS13-vWF axis in disseminated intravascular coagulation: Platelet count/vWF:Ag ratio as a strong prognostic marker. *International journal of laboratory hematology* **44**, 595-602
24. Ma, W. H., Sheng, L., Gong, H. P., Guo, L. L., and Lu, Q. H. (2014) The application of vWF/ADAMTS13 in essential hypertension. *International journal of clinical and experimental medicine* **7**, 5636-5642
25. Chung, D. W., Platten, K., Ozawa, K., Adili, R., Pamir, N., Nussdorfer, F., St John, A., Ling, M., Le, J., Harris, J., Rhoads, N., Wang, Y., Fu, X., Chen, J., Fazio, S., Lindner, J. R., and López, J. A. (2023) Low-density lipoprotein promotes microvascular thrombosis by enhancing von Willebrand factor self-association. *Blood* **142**, 1156-1166
26. Gogia, S., and Neelamegham, S. (2015) Role of fluid shear stress in regulating VWF structure, function and related blood disorders. *Biorheology* **52**, 319-335
27. Kraus, E., Kraus, K., Obser, T., Oyen, F., Klemm, U., Schneppenheim, R., and Brehm, M. A. (2014) Platelet-free shear flow assay facilitates analysis of shear-dependent functions of VWF and ADAMTS13. *Thrombosis research* **134**, 1285-1291
28. Coburn, L. A., Damaraju, V. S., Dozic, S., Eskin, S. G., Cruz, M. A., and McIntire, L. V. (2011) GPIbα-vWF rolling under shear stress shows differences between type 2B and 2M von Willebrand disease. *Biophysical journal* **100**, 304-312
29. Reininger, A. J. (2008) VWF attributes--impact on thrombus formation. *Thrombosis research* **122 Suppl 4**, S9-13
30. Di Stasio, E., and De Cristofaro, R. (2010) The effect of shear stress on protein conformation: Physical forces operating on biochemical systems: The case of von Willebrand factor. *Biophysical chemistry* **153**, 1-8
31. Angeli, V., and Lim, H. Y. (2023) Biomechanical control of lymphatic vessel physiology and functions. *Cellular & molecular immunology* **20**, 1051-1062
32. Paddillaya, N., Mishra, A., Kondaiah, P., Pullarkat, P., Menon, G. I., and Gundiah, N. (2019) Biophysics of Cell-Substrate Interactions Under Shear. *Frontiers in cell and developmental biology* **7**, 251
33. Santhanakrishnan, A., and Miller, L. A. (2011) Fluid dynamics of heart development. *Cell biochemistry and biophysics* **61**, 1-22

 doi:10.20944/preprints202502.0915.v1

34. Jiang, Y., Fu, H., Springer, T. A., and Wong, W. P. (2019) Electrostatic Steering Enables Flow-Activated Von Willebrand Factor to Bind Platelet Glycoprotein, Revealed by Single-Molecule Stretching and Imaging. *J Mol Biol* **431**, 1380-1396
35. Müller, J. P., Mielke, S., Löf, A., Obser, T., Beer, C., Bruetzel, L. K., Pippig, D. A., Vanderlinden, W., Lipfert, J., Schneppenheim, R., and Benoit, M. (2016) Force sensing by the vascular protein von Willebrand factor is tuned by a strong intermonomer interaction. *Proceedings of the National Academy of Sciences of the United States of America* **113**, 1208-1213
36. Wu, T., Yago, T., Lou, J., Yang, J., Miner, J., Coburn, L., López, J. A., Cruz, M. A., McIntire, L. V., McEver, R. P., and Zhu, C. (2008) Platelet glycoprotein Ibα forms catch bonds with WT VWF but not with type 2B von Willebrand disease VWF. *Biorheology* **45**, 72-73
37. Posch, S., Aponte-Santamaría, C., Schwarzl, R., Karner, A., Radtke, M., Gräter, F., Obser, T., König, G., Brehm, M. A., Gruber, H. J., Netz, R. R., Baldauf, C., Schneppenheim, R., Tampé, R., and Hinterdorfer, P. (2017) Mutual A domain interactions in the force sensing protein von Willebrand factor. *J Struct Biol* **197**, 57-64
38. Arce, N. A., Cao, W. P., Brown, A. K., Legan, E. R., Wilson, M. S., Xu, E. R., Berndt, M. C., Emsley, J., Zhang, X. F., and Li, R. H. (2021) Activation of von Willebrand factor via mechanical unfolding of its discontinuous autoinhibitory module. *Nat Commun* **12**
39. Zeng, J. W., Shu, Z. M., Liang, Q., Zhang, J., Wu, W. M., Wang, X. F., and Zhou, A. W. (2022) Structural basis of von Willebrand factor multimerization and tubular storage. *Blood* **139**, 3314-3324
40. Zhang, Q., Zhou, Y. F., Zhang, C. Z., Zhang, X. H., Lu, C. F., and Springer, T. A. (2009) Structural specializations of A2, a force-sensing domain in the ultralarge vascular protein von Willebrand factor. *P Natl Acad Sci USA* **106**, 9226-9231
41. Wang, Y., Morabito, M., Zhang, X. F., Webb, E., Oztekin, A., and Cheng, X. H. (2019) Shear-Induced Extensional Response Behaviors of Tethered von Willebrand Factor. *Biophysical journal* **116**, 2092-2102
42. Jiang, Y., Fu, H. X., Springer, T. A., and Wong, W. P. (2019) Electrostatic Steering Enables Flow-Activated Von Willebrand Factor to Bind Platelet Glycoprotein, Revealed by Single-Molecule Stretching and Imaging. *J Mol Biol* **431**, 1380-1396
43. Ouyang, M. X., Sun, J., Chien, S., and Wang, Y. X. (2008) Determination of hierarchical relationship of Src and Rac at subcellular locations with FRET biosensors. *P Natl Acad Sci USA* **105**, 14353-14358
44. Ouyang, M. X., Zhou, B. Q., Li, C. M., and Deng, L. H. (2024) Characterization of PDGF-Induced Subcellular Calcium Regulation through Calcium Channels in Airway Smooth Muscle Cells by FRET Biosensors. *Biosensors-Basel* **14**
45. Tan, E. V., Chin, C. S. H., Lim, Z. F. S., and Ng, S. K. (2021) HEK293 Cell Line as a Platform to Produce Recombinant Proteins and Viral Vectors. *Front Bioeng Biotech* **9**
46. Zhang, C. J., Kelkar, A., and Neelamegham, S. (2019) von Willebrand factor self-association is regulated by the shear-dependent unfolding of the A2 domain. *Blood Adv* **3**, 957-968
47. Qin, Q., Laub, S., Shi, Y. W., Ouyang, M. X., Peng, Q., Zhang, J., Wang, Y. X., and Lu, S. Y. (2019) for Ratiometric and High-Throughput Live-Cell Image Visualization and Quantitation. *Front Phys-Lausanne* **7**
48. Stockschlaeder, M., Schneppenheim, R., and Budde, U. (2014) Update on von Willebrand factor multimers: focus on high-molecular-weight multimers and their role in hemostasis. *Blood Coagul Fibrin* **25**, 206-216
49. Arisz, R. A., de Vries, J. J., Schols, S. E. M., Eikenboom, J. C. J., de Maat, M. P. M., and Consortium. (2022) Interaction of von Willebrand factor with blood cells in flow models: a systematic review. *Blood Adv* **6**, 3979-3990
50. Ouyang, M. X., Lu, S. Y., Li, X. Y., Xu, J., Seong, J., Giepmans, B. N. G., Shyy, J. Y. J., Weiss, S. J., and Wang, Y. X. (2008) Visualization of polarized membrane type 1 matrix metalloproteinase activity in live cells by fluorescence resonance energy transfer imaging. *J Biol Chem* **283**, 17740-17748
51. Hui Li, Jia G., Yujie Xing, · Linhong Deng,· Mingxing Ouyang. (2024) FRET verifcation of crucial interaction sites in RhoA regulation mediated by RhoGDI. *Med-X* **2**
52. Bergal, H. T., Jiang, Y., Yang, D. R., Springer, T. A., and Wong, W. P. (2022) Conformation of von Willebrand factor in shear flow revealed with stroboscopic single-molecule imaging. *Blood* **140**, 2490-2499

 doi:10.20944/preprints202502.0915.v1

53. He, Z. C., Li, F., Zuo, P., and Tian, H. (2023) Principles and Applications of Resonance Energy Transfer Involving Noble Metallic Nanoparticles. *Materials* **16**
54. Konkle, B. A., Shapiro, A. D., Quon, D. V., Staber, J. M., Kulkarni, R., Ragni, M. V., Chhabra, E. S., Poloskey, S., Rice, K., Katragadda, S., Fruebis, J., and Benson, C. C. (2020) BIVV001 Fusion Protein as Factor VIII Replacement Therapy for Hemophilia A. *New Engl J Med* **383**, 1018-1027
55. Chhabra, E. S., Liu, T. Y., Kulman, J., Patarroyo-White, S., Yang, B. Y., Lu, Q., Drager, D., Moore, N., Liu, J. Y., Holthaus, A. M., Sommer, J. M., Ismail, A., Rabinovich, D., Liu, Z., van der Flier, A., Goodman, A., Furcht, C., Tie, M., Carlage, T., Mauldin, R., Dobrowsky, T. M., Liu, Z. Q., Mercury, O., Zhu, L., Mei, B., Schellenberger, V., Jiang, H. Y., Pierce, G. F., Salas, J., and Peters, R. (2020) BIVV001, a new class of factor VIII replacement for hemophilia A that is independent of von Willebrand factor in primates and mice. *Blood* **135**, 1484-1496
56. Martin, C. M., L. D.; Cruz, M. A. (2007) Purified A2 Domain of von Willebrand Factor Binds to the Active Conformation of von Willebrand Factor and Blocks the Interaction with Platelet Glycoprotein Ibα. *J. Thromb. Haemost.* **5**, 1363-1370
57. Ying, J. L., Y.; Westfield, L. A.; Sadler, J. E.; Shao, J.-Y. (2010) Unfolding the A2 Domain of Von Willebrand Factor with the Optical Trap. *Biophysical journal* **98**, 1685-1693
58. Zhang, X. H., K.; Zhang, C.-Z.; Wong, W. P.; Springer, T. A. (2009) Mechanoenzymatic Cleavage of the Ultralarge Vascular Protein von Willebrand Factor. *Sciencce* **324**, 1330-1334
59. Lynch, C. J., Cawte, A. D., Millar, C. M., Rueda, D., and Lane, D. A. (2017) A common mechanism by which type 2A von Willebrand disease mutations enhance ADAMTS13 proteolysis revealed with a von Willebrand factor A2 domain FRET construct. *Plos One* **12**